Research Article

EASL EUROPEAN ASSOCIATION FOR THE STUDY OF THE LIVER | JOURNAL OF HEPATOLOGY

A hedgehog survival pathway in 'undead' lipotoxic hepatocytes

Keisuke Kakisaka, Sophie C. Cazanave, Nathan W. Werneburg, Nataliya Razumilava, Joachim C. Mertens, Steve F. Bronk, Gregory J. Gores*

Division of Gastroenterology and Hepatology, College of Medicine, Mayo Clinic, Rochester, MN, United States

Background & Aims: Ballooned hepatocytes in non-alcoholic steatohepatitis (NASH) generate sonic hedgehog (SHH). This observation is consistent with a cellular phenotype in which the cell death program has been initiated but cannot be executed. Our aim was to determine whether ballooned hepatocytes have potentially disabled the cell death execution machinery, and if so, can their functional biology be modeled *in vitro*.

Methods: Immunohistochemistry was performed on human NASH specimens. *In vitro* studies were performed using HuH-7 cells with shRNA targeted knockdown of caspase 9 (shC9 cells) or primary hepatocytes from *caspase* $3^{-/-}$ mice.

Results: Ballooned hepatocytes in NASH display diminished expression of caspase 9. This phenotype was modeled using shC9 cells; these cells were resistant to lipoapoptosis by palmitate (PA) or lysophosphatidylcholine (LPC) despite lipid droplet formation. During lipid loading by either PA or LPC, shC9 cells activate JNK which induces SHH expression via AP-1. An autocrine hedgehog survival signaling pathway was further delineated in both shC9 and *caspase* $3^{-/-}$ cells during lipotoxic stress.

Conclusions: Ballooned hepatocytes in NASH downregulate caspase 9, a pivotal caspase executing the mitochondrial pathway of apoptosis. Hepatocytes engineered to reduce caspase 9 expression are resistant to lipoapoptosis, in part, due to a hedgehog autocrine survival signaling pathway.

Keywords: Caspase 3; c-Jun-N-terminal kinase (JNK); Lipoapoptosis; Lysophosphatidylcholine; Palmitate.

Received 30 March 2012; received in revised form 11 May 2012; accepted 21 May 2012, available online 26 May 2012

* Corresponding author. Address: College of Medicine, Mayo Clinic, 200 First Street SW, Rochester, MN 55905, United States. Tel.: +1 507 284 0686; fax: +1 507 284 0762.

E-mail address: gores.gregory@mayo.edu (G.J. Gores).

Abbreviations: NASH, non-alcoholic steatohepatitis; SHH, sonic hedgehog; FFA, free fatty acids; PA, palmitate; LPC, lysophosphatidylcholine; JNK, c-Jun N-terminal kinase; shRNA, short-hairpin RNA; MPH, mouse primary hepatocytes; D-API, 4′,6-diamidine-2′-phenylindole dihydrochloride; EMSA, electrophoretic mobility shift assay; ChIP, chromatin immunoprecipitation; OA, oleate; $C3^{-/-}$, caspase 3 genetic knockout; AP-1, activator protein-1; ACOX-1, acyl-CoA oxidase 1, palmitoyl; CPT, carnitine palmitoyltransferase; ACACA, acetyl-CoA carboxylase alpha; ACACB, acetyl-CoA carboxylase beta.

Introduction

Human hepatocellular injury is ubiquitous due to the prevalence of steatohepatitis syndromes, viral hepatitis, immune mediated insults, genetic diseases, etc. [1]. In these hepatic diseases, hepatocyte fate is often modeled as a binary process – cells either survive or die to be replaced by liver regenerative processes [2]. Yet, cells may resist cell death by downregulating or inhibiting cell death programs, thereby surviving in an altered state. This new cell fate does not merely reflect an escape from death, but rather results in the formation of a unique, functional cell phenotype. The cell phenotype of non-lethal cell injury has been best characterized in model systems where it has been termed the 'undead cell' [3,4]. Because cell death by proapoptotic stimuli requires activation of executioner caspases [5], the undead cell can be engineered by deletion of these downstream caspases. For example, in *Drosophila melanogaster* genetic deletion of the executioner caspase DrICE or Dcp-1 results in a cell type in which otherwise toxic stimuli activate alternative cell signaling cascades producing signals which enhance tissue remodeling [3,4,6].

A candidate undead cell in the liver is the ballooned hepatocyte in non-alcoholic steatohepatitis (NASH). Ballooned hepatocytes are thought to be important in the pathogenesis of NASH and the presence of such cells is used to score disease severity [7,8]. Little is known about ballooned hepatocytes other than they are enlarged cells which have lost cell polarity, frequently contain Mallory–Denk bodies, store neutral triglycerides, contain oxidized phospholipids, no longer stain for cytokeratin 18, and generate the ligand sonic hedgehog [8–10]. The seminal work by Diehl and colleagues demonstrating sonic hedgehog (SHH) generation by ballooned hepatocytes suggests this cell may, in fact, be a functional cell with an altered phenotype [8,11]. For example, in *D. melanogaster* retinal cells in which the cell death program is initiated but cannot be executed also generate SHH [6]. The mechanisms by which undead cells continue to evade cell death remain elusive, but given the potency of SHH as a survival factor, it is possible that this ligand serves as an autocrine survival factor.

Herein, we demonstrate that ballooned cells have reduced expression of a potent downstream caspase, caspase 9, suggesting they may not efficiently execute cell death pathways. To understand the functional implications of this observation, we modeled lipotoxic stress in HuH-7 cells in which caspase 9 had been knocked down by short hairpin RNA technology (shC9 cells). Knockdown of caspase 9 protected hepatocytes from lipotoxicity by the saturated free fatty acid (FFA), palmitate (PA) or the

phospholipid lysophosphatidylcholine (LPC). Interestingly, PA or LPC treated shC9, but not wild type cells, generate sonic hedgehog by a c-Jun-N-terminal kinase (JNK)-dependent pathway. Blockade of hedgehog signaling resulted in cell death of shC9 cells following exposure to lipotoxic agents. Similar observations were confirmed in primary *caspase* $3^{-/-}$ mouse hepatocytes. We speculate that these engineered cells model the functional phenotype of ballooned hepatocytes, albeit not the specific morphology, and, in turn, support the concept of ballooned hepatocytes as an altered, but functional cell population which has escaped cell death.

Materials and methods

Immunohistochemistry (IHC)

Formalin-fixed, paraffin-embedded liver sections (5 μm thick) from three patients with non-alcoholic steatohepatitis (NASH) were obtained following approval by the Institutional Review Board (IRB), Mayo Clinic, Rochester MN, USA. In conjunction with the clinical core of P30DK084576, the sections were pre-selected by an experienced hepatopathologist for their abundance of ballooned hepatocytes. These sections were deparaffinized in xylene and rehydrated through graded alcohols. After tissue permeabilization in 0.1% Triton X100 for 2 min, antigen retrieval was performed by incubation in sodium citrate buffer (0.01 M sodium citrate, 0.05% Tween 20; pH 6.0) for 30 min utilizing a vegetable steamer. Samples were cooled down, and endogenous peroxidase activity was quenched by incubation for 15 min in 3% H_2O_2 (diluted in deionized H_2O). Sections were washed in changes of phosphate-buffered saline (PBS), three times for 5 min. The VECTASTAIN Elite ABC and ImmPACT VIP peroxidase substrate kits (Vector laboratories, Burlingame, CA, USA) were used in further steps according to manufacturer's instructions. After blocking non-specific binding for 1 h, sections were incubated with anti-caspase-9 p10 (F-7) mouse monoclonal primary antibodies (1:50; sc-17784) or anti-caspase-2_L (C-20) goat monoclonal primary antibodies (1:50; sc-626-G, Santa Cruz Biotechnology, Santa Cruz, CA, USA) for 30 min at room temperature. Prior to mounting, the sections were counterstained with hematoxylin for 3 min (Sigma–Aldrich, St. Louis, MO, USA). Samples were examined with light microscopy. Analysis of at least 20 cells of each type from each patient was conducted using Image J version 1.44 software (NIH, Bethesda, MD, USA). Ballooned cells were confirmed in hematoxylin and eosin (H&E) stained sections.

Cells

HuH-7 cells, a human hepatocellular carcinoma cell line, were maintained in Dulbecco's modified Eagle's medium containing glucose (25 mM) supplemented with 10% fetal bovine serum, 100,000 IU/L penicillin and 100 mg/L streptomycin. We also employed HuH-7 cells stably expressing a short-hairpin RNA (shRNA) targeting caspase 9, shC9 cells. Mouse primary hepatocytes (MPH) were isolated from C57BL/6 wild type (Jackson Laboratory, Bar Harbor, ME, USA) and *caspase* $3^{-/-}$ mice by collagenase perfusion and plated as primary cultures [12]. Development and characterization of the *caspase* $3^{-/-}$ mice has been previously reported [13]. MPH were maintained in Waymouth medium supplemented with 10% fetal bovine serum, 100,000 IU/L penicillin, 100 mg/L streptomycin, and 100 nM insulin.

Phase contrast, fluorescent and confocal microscopy

HuH-7 cells and shC9 cells were grown on glass bottom culture dishes for phase contrast and fluorescence microscopy, or glass coverslips for confocal microscopy. The following studies were conducted in conjunction with the microscopy core of the P30DK084567. For live cell imaging, lipid droplets were fluorescently labeled by incubation with 100 μg/ml of Bodipy 505/515 (Invitrogen, Camarillo, CA, USA) for 1 min at 37 °C. Identical cells were viewed using phase contrast and then fluorescent optics on a Zeiss Axiovert 200 epifluorescent microscope (Zeiss, Thornwood, NJ, USA). Fluorescence was visualized using excitation and emission wavelengths of 488 and 507 nm, respectively. Both phase contrast and fluorescent digital images were acquired and analyzed using a cooled-CCD Orca II camera (Hamamatsu Photonics, Hamamatsu City, Japan) with IPLab software (Scanalytics, Fairfax, VA, USA). Fluorescent lipid droplet area as a percent of the total cellular area was quantified using Image J version 1.44 software (NIH, Bethesda, MD, USA).

In separate studies, cells were fixed with 3% paraformaldehyde for 30 min at room temperature [14]. Intracellular lipid droplets were labeled with 10 μg/ml of Bodipy 505/515 for 10 min at room temperature, and mounted in Prolong Antifade mounting media (Invitrogen, Camarillo, CA, USA). Lipid droplet fluorescence intensity per cell was quantified using an inverted phase/fluorescence microscope (Axiovert 35M; Carl Zeiss, Inc., Thornwood, NY, USA) and Metafluor quantitative fluorescence imaging software from Universal Imaging Corp. (West Chester, PA, USA) [15]. For confocal microscopy, cells were fixed and labeled as described above and visualized using an inverted laser-scanning confocal microscope (Zeiss LSM 510, Carl Zeiss, Jena, Germany) with excitation and emission wavelengths of 488 and 507 nm, respectively.

For SHH or ubiquitin immunocytochemistry, cells plated on coverslips were fixed with 4% paraformaldehyde in PBS for SHH staining or with cold acetone on dry ice for ubiquitin staining, respectively, and permeabilized with 0.0125% (w/v) CHAPS in PBS for both stainings. The primary antiserum was rabbit anti-SHH (sc-9024, Santa Cruz Biotechnology, Santa Cruz, CA, USA) at a dilution of 1:300 or rabbit anti-ubiquitin (Z0458, Dako, Carpinteria, CA, USA) at a dilution of 1:500. The secondary antiserum was Alexa Fluor 488-conjugated or 568-conjugated anti-rabbit IgG (Molecular Probes, Eugene, OR, USA), and ProLong Antifade with DAPI (Molecular Probes) was used as mounting medium. Images were acquired by confocal microscopy employing excitation and emission wavelengths of 488 and 507 nm for SHH staining or excitation and emission wavelengths of 558 and 583 nm for ubiquitin staining. Cells with positive immunoreactivity for the active conformation of SHH or cells with ubiquitin-punctate staining, respectively, were counted and expressed as a percentage of total cells.

Electrophoretic mobility shift assay (EMSA)

EMSA was performed as previously described by us in detail [16]. Briefly, nuclear extracts from shC9 cells were prepared using NE-PER nuclear and cytoplasmic extraction reagents (Pierce Biotechnology, Rockford, IL, USA) according to the manufacturer's instructions. For the EMSA, 20 μg of nuclear proteins was incubated at room temperature for 20 min in binding buffer (25 mM HEPES, pH 7.5, 0.1 M NaCl, 2 mM EDTA, 6% glycerol, 0.1% Triton X-100, 0.1 mM phenylmethylsulfonyl fluoride, 0.4 mM dithiothreitol, 0.5 μg/μl poly(dI-dC), 0.5 μg/μl salmon sperm) with 0.04 pmol of CY 5.5-labeled double-stranded DNA oligonucleotides containing either one of the putative activator protein-1 (AP-1) binding sequences (BS1) or (BS2). Each sequence with the mutated putative AP-1 binding sequence (mutant BS1 or mutant BS2) was also employed as a negative control (Supplementary Table 1). Protein-DNA complexes were separated from the unbound DNA probe by electrophoresis through 5% native polyacrylamide gels containing 0.5x Tris borate-EDTA. Fluorescence was visualized directly on the gel using an Odyssey fluorescent imager (Licor Biosciences, Lincoln, NE, USA). For competition assays, a 200-fold molar excess of unlabeled double-stranded oligonucleotide was added to the reaction mixture 20 min before the addition of the fluorescent probe. In the supershift assays, nuclear cell extract was first incubated at room temperature for 25 min with 2 μg of anti-phospho-c-Jun antibody (Santa Cruz Biotechnology). The entire antibody/protein mixture was then incubated with CY 5.5-labeled probe and processed for the gel shift as described above.

Chromatin immunoprecipitaion (ChIP) assay

ChIP assays were performed employing shC9 (6–10 million cells) using a commercially available assay (Active Motif, Carlsbad, CA, USA) according to the manufacturer's instructions [17]. Briefly, shC9 cells were treated for 6 h with 800 μM palmitate or for 4 h with 85 μM LPC; the cells were then fixed with 1% formaldehyde in PBS at room temperature for 10 min. The formaldehyde crosslinking reaction was quenched with 125 mM glycine, the cells were lysed, and chromatin was sheared into small and uniform fragments by an enzymatic reaction. Following centrifugation, the DNA concentration in the supernatant was quantified by measuring absorbance at 260 nm. Samples containing 30 μg of DNA were next incubated with Protein G magnetic beads, ChIP Buffer 1, Protease Inhibitor Cocktail, the phospho-c-Jun antibody at 2 μg and dH_2O at 4 °C overnight. The immune complex was separated from the sample buffer by a magnetic stand and washed sequentially with ChIP Buffer1 and ChIP Buffer 2. The sample was next eluted with Elution Buffer AM2 and then added to the Reverse Cross-linking Buffer and heated at 95 °C for 15 min. The proteins were digested by proteinase K, and the DNA in the ChIP sample was used as template for quantitative real-time PCR. The primers used in this assay are depicted in Supplementary Table 2.

Immunoblot analysis

Whole cell lysates were prepared as previously described [12]. Nuclear cell extracts were prepared using NE-PER nuclear and cytoplasmic extraction reagents (Pierce Biotechnology, Rockford, IL, USA) according to the manufacturer's instructions. An equal amount of protein (50–80 μg) was resolved by SDS–PAGE on a 12.5–18% acrylamide gel, transferred to nitrocellulose membranes, and incubated with primary antibodies. Membranes were incubated with appropriate horseradish peroxidase-conjugated secondary antibodies (Biosource International, Camarillo, CA, USA). The bound antibody was visualized using a chemiluminescent substrate (ECL; Amersham, Arlington Heights, IL, USA) and exposure to Kodak X-OMAT film (Eastman Kodak, Rochester, NY, USA).

Materials and methods for treatment of hepatocytes with lipids, quantitation of cell death, and quantititative real-time PCR, Gli reporter assay, antibodies and reagents, and statistics are included in the Supplementary data.

Results

Ballooned hepatocytes in NASH display reduced caspase 9 expression

Loss of executioner caspase function is sufficient to prevent cell death in developmental systems. Therefore, we performed immunohistochemistry in human NASH specimens for caspase 9, a potent executioner caspase. Ballooned hepatocytes, but not neighboring hepatocytes, displayed diminished caspase 9 expression (Fig. 1A). In contrast, expression of the upstream caspase 2 was readily identified in ballooned hepatocytes (Fig. 1A). Caspase 2 has a long prodomain similar to caspase 9, and therefore, served as a control for a caspase of similar size as caspase 9. These suggest ballooned hepatocytes are not merely damaged cells on the path to cellular demise, but likely are functional cells which have downregulated cell death pathways.

Diminished cell death in hepatocytes deficient in caspase 9 or 3 despite lipid droplet accumulation

We sought to model the ballooned hepatocyte phenotype with downregulation of caspase 9, and therefore, generated shC9 HuH-7 cells (shC9 cells) (Fig. 1B). As assessed by phase contrast morphology, the shC9 cells did not appear different from the parent cell line. The shC9 cells (Fig. 1C), however, actually demonstrated more robust lipid droplet formation as compared to wild type cells following incubation with oleate (OA) or palmitate (PA) (Fig. 1C and D). The enhanced lipid loading of shC9 cells could not be explained by decreased lipolysis as expression of the rate limiting enzyme for lipolysis[18,19], acyl-CoA oxidase 1, palmitoyl (ACOX-1), or β-oxidation, carnitine palmitoyltransferase 1A and 2 (CPT-1A and -2), acetyl-CoA carboxylase alpha (ACACA) and acetyl-CoA carboxylase beta (ACACB) was not downregulated in these cells (Supplementary Fig. 1). Rather enhanced lipid droplet accumulation by shC9 cells likely reflects their ability to resist lipoapoptosis by free fatty acids allowing further lipid accumulation over time. As the saturated free fatty acid PA induces lipoapoptosis via a metabolite lysophosphatidylcholine (LPC) [12], we quantified apoptosis in shC9 and wild type cells using both PA and LPC. Using either lipotoxic agent, shC9 cells were more resistant to PA or LPC cytotoxicity (Supplementary Fig. 2A–C). To confirm these results in primary hepatocytes, we employed hepatocytes from wild type and caspase 3 deficient ($C3^{-/-}$) mice. We posited that, given the dominant role of caspase 3 as an executioner caspase downstream of caspase 9, these cells may also be resistant to lipotoxicity (Supplementary Fig. 3B), and indeed, they were apoptosis resistant, despite lipid droplet accumulation (Supplementary Fig. 3A). Finally, because ballooned hepatocytes in the NASH liver display enhanced ubiquitin chain accumulation [20], we performed immunocytochemistry for ubiquitin chains following PA treatment. shC9 cells manifest increased punctate ubiquitin staining following PA treatment, further suggesting their phenotypic similarity to ballooned hepatocytes (Supplementary Fig. 4). Taken together, these data demonstrate that knockdown or deletion of caspases downstream of mitochondrial dysfunction results in cells resistant to lipoapoptosis in spite of lipid droplet accumulation and ubiquitin chain accumulation. However, we note that these cells do not completely model the ballooned cellular morphology observed in human NASH.

PA and LPC induce SHH expression in lipoapoptosis resistant hepatocytes by a JNK-dependent pathway

Next, we examined SHH generation by shC9 cells subjected to lipotoxic stress by PA or LPC. shC9 and *caspase* $3^{-/-}$, but not wild type HuH-7 cells, expressed SHH at both mRNA and protein level following treatment with either PA or LPC (Fig. 2A–C). In *D. melanogaster*, the undead cell phenotype requires activation of initiator caspases which induce alternative signaling pathways in the absence of downstream caspases [3,4]. Therefore, we next explored the effect of the pan-caspase inhibitor Z-VAD-fmk on SHH generation by shC9 cells treated with PA or LPC. Z-VAD-fmk treatment blunted SHH expression in shC9 cells exposed to either PA or LPC (Fig. 3A). During lipoapoptosis, c-Jun N-terminal kinase (JNK) activation occurs by a mechanism downstream of caspase 8 activity [12,17,21]. Consistent with this information, Z-VAD-fmk treatment reduced phosphorylation of c-Jun, a JNK substrate, during incubation of shC9 cells with PA or LPC (Fig. 3B). As lipotoxic stress is associated with death receptor 5-dependent activation of caspase 8 [22], presumably Z-VAD-fmk is inhibiting this initiator caspase. To determine whether JNK activation directly contributes to SHH expression during lipotoxic stress, we employed the pharmacological JNK inhibitor SP600125. SP600125, at a concentration which blocks c-Jun phosphorylation, reduced SHH expression in this model (Fig. 3C and D). Collectively, these observations implicate JNK activation in the generation of SHH in hepatocytes resistant to apoptosis.

Activator protein-1 (AP-1) mediates SHH transcription during lipotoxic stress

Phosphorylated c-Jun heterodimerizes with other proteins to form the AP-1 transcription factor complex [23]. To ascertain if AP-1 may directly upregulate SHH transcription, computational analysis of the human *SHH* gene sequence was performed to identify consensus AP-1 binding sites. Two putative AP-1 binding sites were identified within the human *SHH* promoter; one at −4525/−4518 (Binding Sequence 1, BS1) and a second at −2608/−2601 (Binding Sequence 2, BS2) (Fig. 3E). To test whether AP-1 complexes bind to these sites, an EMSA was performed using CY5.5-labeled oligonucleotide probes for each putative binding site (Supplementary Table 1). Using nuclear extracts obtained from either PA or LPC treated shC9 cells, protein binding to both BS1 and BS2 was observed (Fig. 3E). This binding was no longer observed when extracts were incubated with anti-phospho-c-Jun antisera, as presumably the antiserum binding to

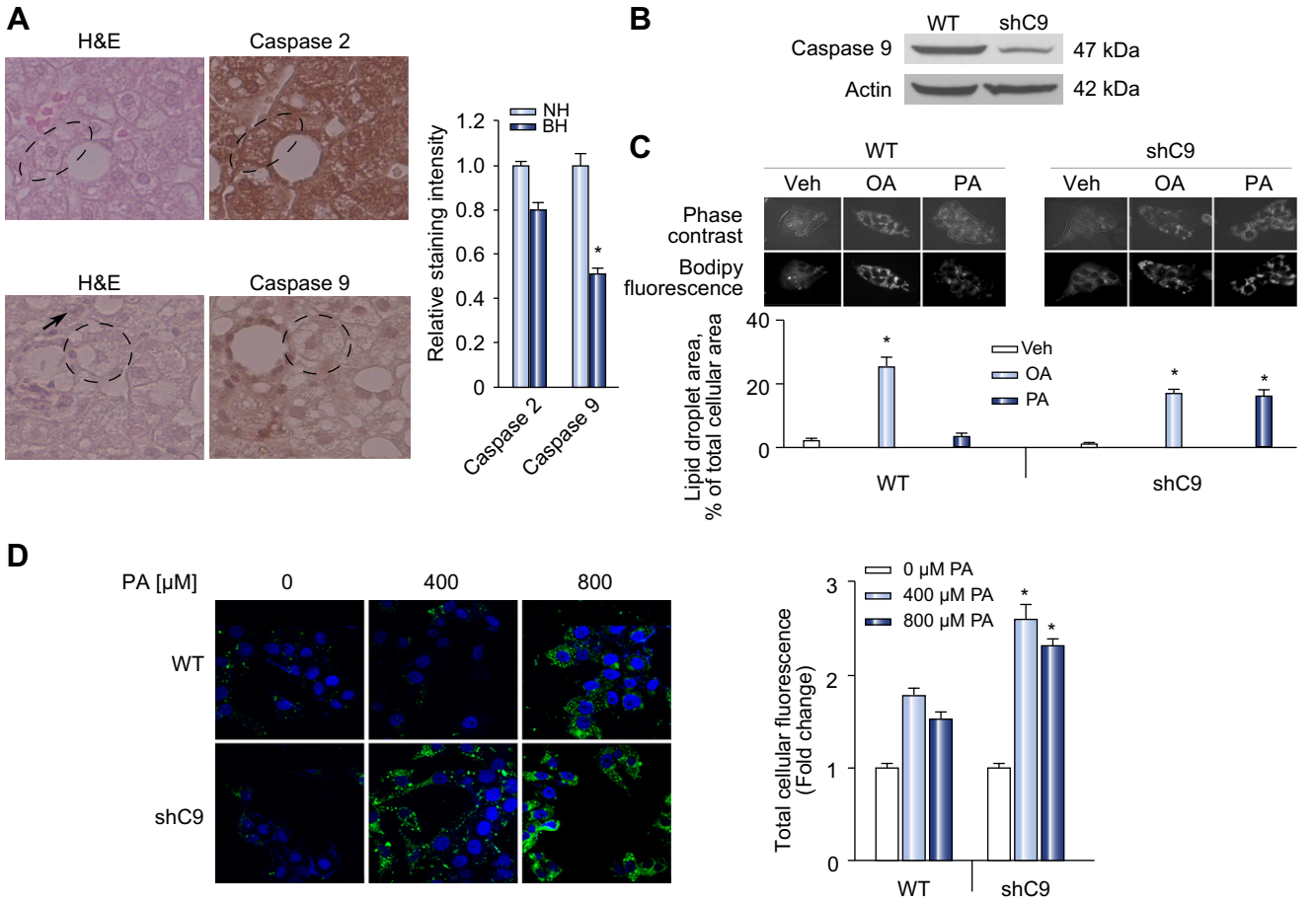

Fig. 1. Ballooned hepatocytes display decreased caspase 9 in NASH specimens; loss of caspase 9 or 3 enhances lipid loading *in vitro*. (A) Ballooned hepatocytes (BH) and non-balloned hepatocytes (NH, arrow) were identified in H&E stained sections (circled cells). Immunohistochemistry for caspase 2 and 9 was performed in sections from the same specimens. Caspase 2 and 9 staining intensity was quantified by NIH Image J software (right panel). Staining intensity of NH was set at 1.0. (B) Whole cell lysates were prepared from wild type (WT) and shC9 cells and immunoblot analysis performed for caspase 9. (C) WT and shC9 cells were incubated with vehicle (Veh), palmitate (PA) or oleate (OA) at 400 μM for 12 h. Lipid droplets were labeled with Bodipy 505/515, and cells imaged by phase contrast microscopy and fluorescent microscopy. Lipid droplet area and total cell area were measured by NIH Image J software. (D) WT and shC9 cells were incubated with PA for 12 h at 0, 400, or 800 μM, respectively, labeled with Bodipy 505/515, and imaged by confocal microscopy. Fluorescence intensity was quantified using Metafluor quantitative software and expressed as fold change over vehicle. All data are expressed as mean ± SEM for at least three experiments; $^{*}p$ <0.01.

AP-1 masks the oligonucleotide binding site; an observation implicating AP-1 in the formation of the protein:oligonucleotide complex. Binding was also no longer observed when extracts were incubated with a 200-fold molar excess of the unlabeled probe, or when using a mutated probe in which the critical AP-1 binding residues had been altered. Finally, to further confirm that AP-1 binds to these promoter sequences of the *SHH* gene, a ChIP assay was performed using the primers listed in Supplementary Table 2. Immunoprecipitation of c-Jun from nuclear extracts obtained from PA- or LPC-treated shC9 cells captured both putative AP-1 binding sequences within the *SHH* promoter (Fig. 3F). In contrast, no binding of c-Jun to an unrelated upstream region of the *SHH* promoter was observed. These data provide evidence for two *bona fide* AP-1 binding sequences within the *SHH* promoter suggesting AP-1 may induce expression of this gene.

SHH provides autocrine survival signals during lipotoxic stress

As critical as caspases are for cell apoptosis, loss of caspase activity often delays but does not abrogate cell death in mammalian cells [24]. Therefore, we anticipated that SHH expression functions as an additional survival factor during lipotoxic stress given its role as a potent survival factor in other systems [6,25–27]. To test this concept, we first looked for active hedgehog signaling in shC9 cells. Following binding of SHH to its cognate receptor Patched, Smoothened is derepressed resulting in translocation of the Gli transcription factors into the nucleus, especially Gli2 [28,29]. Indeed, Gli2 translocation into nuclear cell fractions was readily identified in PA- and LPC-treated shC9 cells (Fig. 4A). Hedgehog signaling in a feed forward manner also increases *Gli2* mRNA expression [29], which was observed in shC9 cells following exposure to PA or LPC (Fig. 4B). To further examine hedgehog signaling, a Gli reporter gene assay was employed. Consistent with the above observations, PA or LPC increased Gli reporter gene activity in shC9 cells (Fig. 4C). These observations identified an autocrine hedgehog signaling pathway in shC9 cells following lipotoxic stress. To explore this concept, shC9 cells were treated either with GANT61 (a Gli1/2 inhibitor) or GDC-0449 (a Smoothened antagonist) followed by exposure to PA or LPC [30]. GANT61 as well as GDC-0449 prevented PA

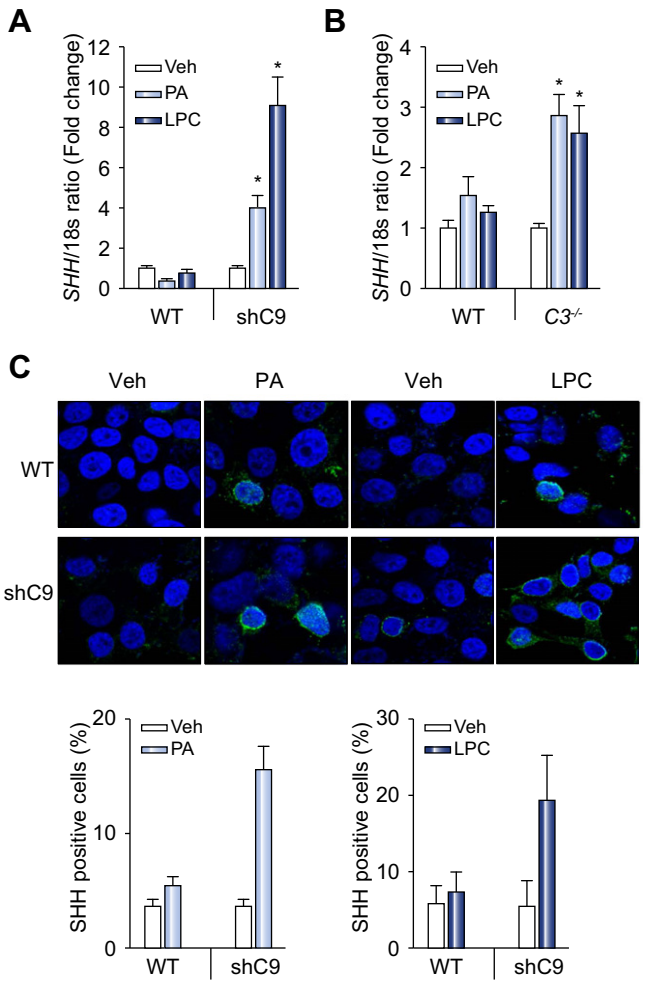

Fig. 2. PA and LPC induce SHH expression in shC9 cells and primary mouse hepatocytes from *caspase 3*$^{-/-}$ animals. (A) Wild type (WT) and shC9 cells were incubated with vehicle (Veh), PA at 800 μM for 16 h, or LPC at 85 μM for 6 h. *SHH* mRNA was quantified by real-time PCR, normalized to *18S* rRNA, and expressed as fold change over vehicle. (B) Mouse primary hepatocytes (MPH) from WT and caspase 3 deficient animals ($C3^{-/-}$) were incubated with Veh, PA (400 μM) for 12 h, or LPC (42.5 μM) for 6 h. *SHH* mRNA was quantified by real-time PCR. (C) WT and shC9 cells were incubated with Veh, PA (800 μM) for 8 h or LPC (85 μM) for 4 h, respectively. Immunofluorescence was performed for SHH and visualized by confocal microscopy; the number of SHH-positive versus total cells is depicted. All data are expressed as mean ± SEM for three experiments; *p <0.01.

and LPC induced *Gli2* mRNA expression and Gli reporter gene activity (Fig. 4B and C). Because shC9 cells were generated from a human hepatoma cell line, HuH-7 cells, we confirmed the above findings in mouse primary hepatocytes. When mouse primary hepatocytes from $C3^{-/-}$ mice were treated with either PA or LPC, *Gli2* mRNA levels increased 4-fold (Supplementary Fig. 5A); furthermore, pretreatment with GANT51 or GDC-0449, followed by exposure to PA or LPC, suppressed this increase in *Gli2* mRNA expression (Supplementary Fig. 5A). Finally, we sought to determine whether this hedgehog autocrine signaling pathway functions as a survival pathway in both shC9 cells and $C3^{-/-}$ hepatocytes subjected to lipotoxic stress. PA and LPC induced lipoapoptosis was enhanced by concurrent treatment with either GANT61 or GDC-0449 in both shC9 cells and $C3^{-/-}$ hepatocytes (Fig. 4D and Supplementary Fig. 5B). Taken together, these observations suggest that lipotoxic stress in hepatocytes evading cell death results in a hedgehog signaling pathway further endowing the cell with potent survival signals.

Discussion

We posited that the ballooned hepatocyte in NASH represents an altered cellular phenotype which has escaped cell death analogous to the 'undead cell' in developmental models. Consistent with this concept, we observed a reduction of caspase 9 protein expression in ballooned hepatocytes. We sought to model this phenotype *in vitro* and explore its functional biology. Our results indicate that during lipotoxic stress by PA or LPC: (1) targeted knockdown of caspase 9 or genetic deficiency of caspase 3 reduces cell death despite accumulation of lipid droplets; (2) surviving cells display an altered phenotype as manifested by JNK-dependent expression of SHH; and (3) an autocrine SHH pathway contributes to cell survival.

The results of this study provide new mechanistic insights regarding the phenotype of hepatocytes undergoing lipotoxic stress without succumbing to cell death, and have implications for the understanding of the functional biology of the ballooned hepatocyte in NASH.

Hepatocyte lipotoxicity involves a complex network of proapoptotic stimuli. Saturated free fatty acids such as palmitate promote formation of plasma membrane subdomains, resulting in death receptor 5 clustering causing activation of caspase 8 [22]. In hepatocytes, caspase 8 cleaves the pro-apoptotic BH3-only protein Bid to form truncated Bid (tBid) which translocates to mitochondria [31]. JNK activation also occurs, facilitating induction of the pro-apoptotic BH3-only protein PUMA [16,17]. The mitochondrial accumulation of BH3-only proteins, tBid, PUMA, and Bim (also upregulated by toxic FFA), results in mitochondrial dysfunction with release of apoptogenic factors from the intermitochondrial membrane space into the cytosol, causing caspase 9 activation. FFAs also induce loss of the anti-apoptotic Bcl-2 protein Mcl-1 [32]. Our findings suggest ballooned hepatocytes have reduced caspase 9 expression (the key caspase initiating apoptosis following mitochondrial dysfunction), and targeted knockdown of caspase 9 represses lipotoxicity *in vitro*. Given the intense dysregulation of Bcl-2 proteins during lipotoxic stress, it is not surprising that surviving cells have disabled the apoptotic machinery downstream of mitochondrial dysfunction. Moreover, these observations are also consistent with the observation in model systems where loss of a downstream caspase activity is cytoprotective and results in an altered cell phenotype. In our current studies, we also observed reduced cell killing despite enhanced neutral lipid accumulation in cells with reduced caspase 9 expression; this observation is consistent with evolving concepts that FFA acids are the toxic instigators of cell death whereas their esterification into neutral lipids is a detoxification process [33–35].

In a series of landmark observations, Anna Mae Diehl and coworkers have demonstrated the importance of hedgehog signaling in liver pathobiology [8,11,20]. For example, they have reported that hedgehog pathway activation parallels disease severity in NASH [8], whereas hedgehog signaling antagonism is antifibrogenic [11]. More importantly, in a pivotal study, they also identified ballooned hepatocytes as a cellular source of SHH in NASH [20]. Our *in vitro* model has implications for these

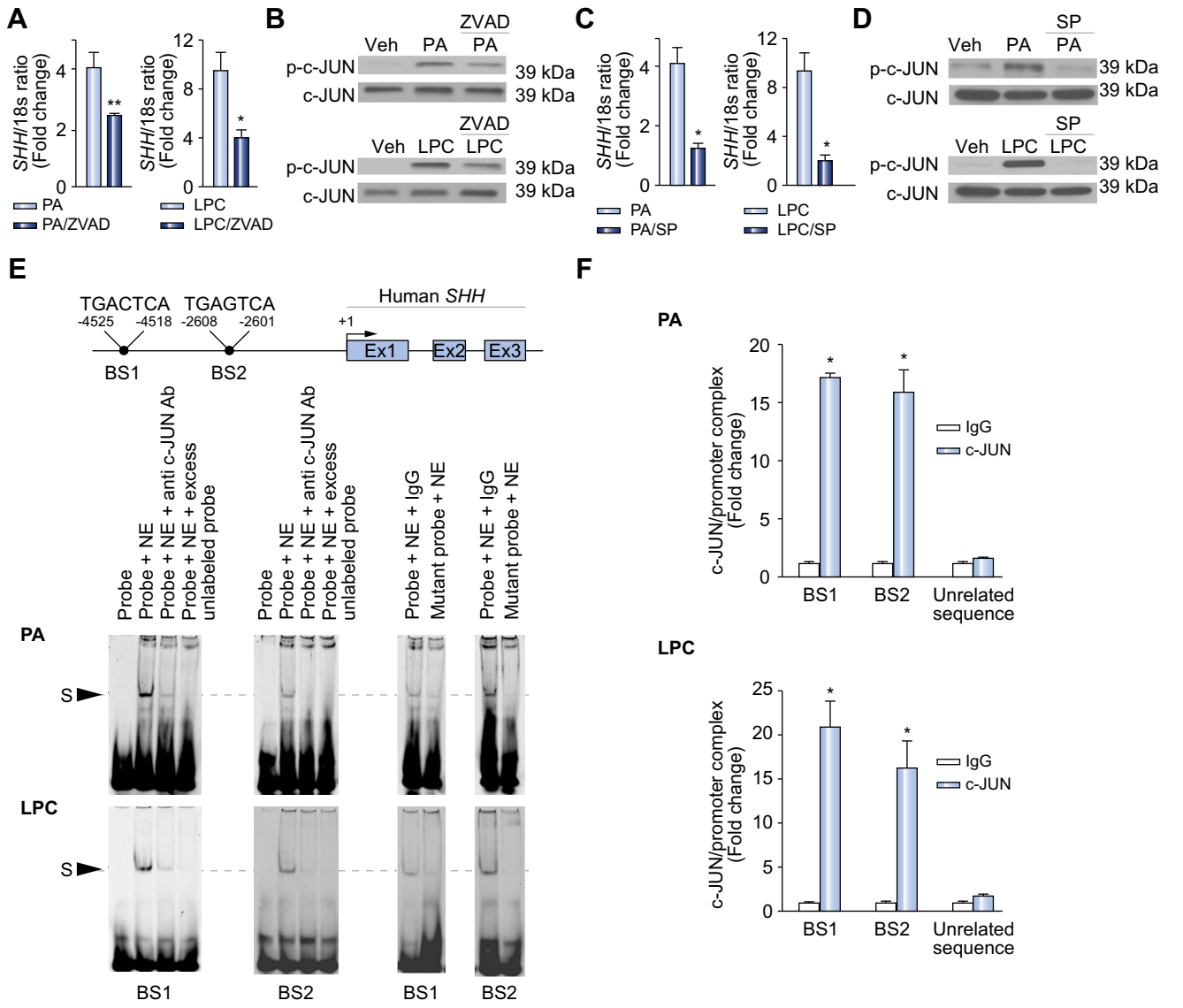

Fig. 3. PA and LPC induce SHH expression via AP-1 mediated transcription. (A) shC9 cells were incubated with PA (800 μM) for 16 h in the absence or presence of the pancaspase inhibitor Z-VAD-fmk (ZVAD, 10 μM) and *SHH* mRNA expression was quantified by real-time PCR. (B) Cells were treated with vehicle (Veh), PA as above or LPC (85 μM) for 8 h. Immunoblot analysis was performed for phospho-c-Jun (p-c-Jun) or total c-Jun using whole cell lysates. (C) shC9 cells were treated with PA as per panel A, in the presence or absence of the JNK inhibitor SP600125 (50 μM), and *SHH* mRNA expression was quantified using real-time PCR. (D) Whole cell lysates were prepared from shC9 cells treated with PA or LPC as above, and immunoblot analysis was performed for p-c-Jun or total c-Jun. (E) The *SHH* gene is depicted along with the two putative AP-1 binding sites (BS1 and BS2). shC9 cells were incubated with PA or LPC as described above. Nuclear protein extracts were isolated and EMSA performed using a CY 5.5-labeled AP-1 probe. Anti-phospho-c-Jun antibodies were used in the supershift experiments. Protein complexes are indicated by arrows (S, shift). No specific retarded complexes were observed when adding 200-fold molar excess of the unlabeled probe or when using the CY 5.5-labeled mutated probe. CY 5.5-labeled probe only was used as a negative control. (F) shC9 cells were incubated with PA or LPC as above. Cells were fixed and lysed, DNA fragments pulled down with p-c-Jun antibody, and the collected DNA subjected to quantitative RT-PCR analysis using primers for BS1 or BS2. DNA fragments pulled down with IgG were used as negative control for the p-c-Jun specific antisera. Primers of unrelated sequence were used as negative control for BS1 or BS2 specific primers. All data are expressed as mean ± SEM for three experiments; $^{*}p$ <0.01, $^{**}p$ <0.05.

studies. We were able to demonstrate, in cells failing to execute the cell death program during lipotoxic insults, that JNK activation induces SHH expression via stimulation of the transcription factor AP-1; indeed, our studies identified two functional binding sites for AP-1 within the *SHH* promoter. Our results parallel those obtained in developmental systems in which stressed cells that cannot fully execute the cell death program display an altered phenotype dependent upon JNK activation and aberrantly express SHH [36,37].

The current study also identified an autocrine hedgehog survival signaling process in shC9 cells during lipotoxic stress. This observation has potential implications for NASH therapy. We speculate that inhibition of hedgehog survival signaling in ballooned hepatocytes would result in their death and elimination from the liver. If ballooned hepatocytes are the main source of SHH in NASH [20], their elimination would also prevent profibrogenic hedgehog signaling within the liver. Finally, our data may also explain the anti-fibrogenic effect of caspase inhibitors

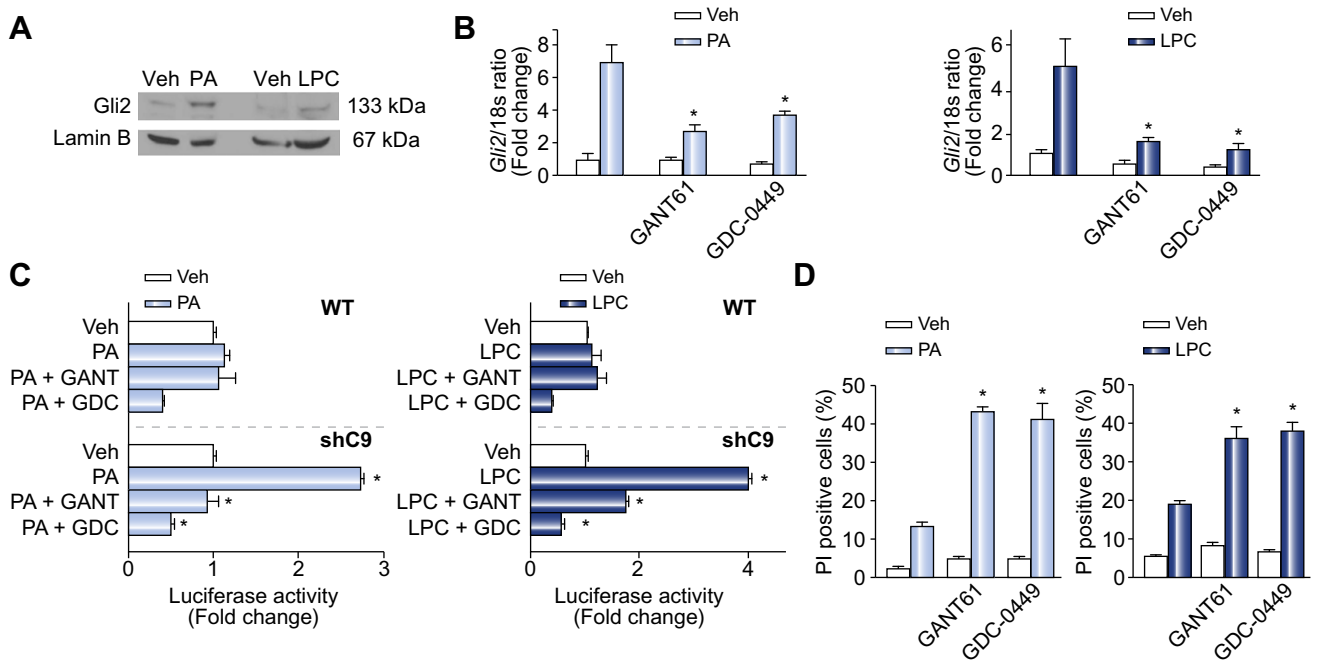

Fig. 4. An autocrine SHH survival pathway in shC9 cells during lipotoxic stress. (A) Nuclear protein extracts were isolated from shC9 cells treated with vehicle (Veh), PA or LPC as described in Fig. 2, and immunoblot analysis performed for Gli2. Lamin B was used as loading control. (B) shC9 HuH-7 cells were preincubated for 24 h with vehicle, the Gli1/2 inhibitor GANT61 (5 μM), or the Smoothened antagonist GDC-0449 (20 μM). After pre-incubation, shC9 HuH-7 cells were incubated with Vehicle (Veh), PA (800 μM) for 16 h or LPC (85 μM) for 6 h. *Gli2* mRNA was quantified by real-time PCR, normalized to 18S rRNA, and expressed as fold change over vehicle. (C) Wild type (WT) and shC9 cells were transiently transfected (16 h) with a reporter construct, containing eight consecutive consensus GLI binding sites (8x-GLI), and co-transfected with pRL-CMV. Cells were preincubated with/without GANT61 or GDC-0049 as described above, and then treated as indicated with PA (800 μM) for 16 h or LPC (85 μM) for 10 h. Cells were lysed and firefly and *Renilla* luciferase activities quantified; data (firefly/*Renilla* luciferase activity) are expressed as fold increase over vehicle-treated cells. (D) After preincubation with GANT61 or GDC-0449, shC9 cells were incubated for 16 h with PA (400 μM) or LPC (42.5 μM), respectively. Cell death was quantified as propidium iodide positive (PI) cells expressed as a percentage of total cell number. All data are expressed as mean ± SEM for three experiments; *p <0.01.

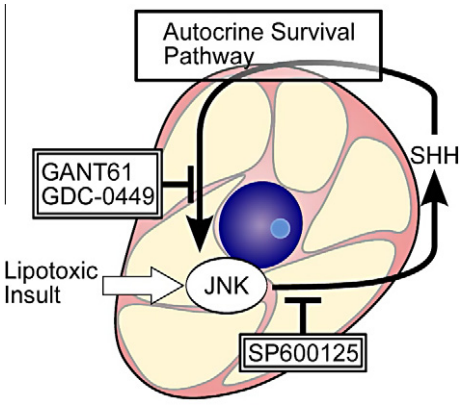

Fig. 5. A schematic model for SHH expression as an autocrine survival factor during lipotoxic stress. Lipotoxic insult-induced AP-1 mediates SHH expression. Blocking JNK signaling with SP600125 represses SHH generation. Inhibition of SHH pathway signaling by either GANT61 or GDC-0449 blocks this autocrine SHH survival pathway in "undead cells", resulting in their cellular demise.

in preclinical studies of NASH since these inhibitors also block SHH expression, a profibrogenic mediator [38].

We provocatively propose that ballooned hepatocytes are cells which have initiated but cannot execute the cell death program due to loss of caspase 9 (Fig. 5). The mechanism(s) responsible for caspase 9 downregulation remain unclear and will require biochemical interrogation of this minor cell population once appropriate techniques can be validated to do so. The recent report of an animal model of NASH with ballooned hepatocytes may aid such studies [39]. Although this *in vitro* model does not replicate the morphology of the ballooned hepatocyte, it does duplicate at least one of the phenotypical characteristics of ballooned hepatocytes, namely SHH generation. Processes in addition to cell death avoidance are apparently required for the ballooned cell morphology.

Financial support

This work was supported by NIH Grants DK41876 to G.J.G., the optical microscopy and clinical cores of P30DK084567, and the Mayo Foundation.

Conflict of interest

The underlying research reported in the study was funded by the NIH Institutes of Health.

Acknowledgements

This work was supported by NIH Grant DK41876 and the optical and microscopy cores of P30DK084567 and the Mayo Foundation. We thank Drs. Christian D. Fingas, Maria E. Guicciardi, Justin L. Mott, and Scott H. Kaufmann for helpful discussions; Dr. Harmeet

Malhi for reading the manuscript and providing insightful comments and suggestions; Eugene W. Krueger for aiding the studies employing contrast microscopy; and Courtney N. Hoover for her excellent secretarial assistance.

Supplementary data

Supplementary data associated with this article can be found, in the online version, at http://dx.doi.org/10.1016/j.jhep.2012.05.011.

References

[1] Malhi H, Gores GJ. Cellular and molecular mechanisms of liver injury. Gastroenterology 2008;134:1641–1654.
[2] Gouw AS, Clouston AD, Theise ND. Ductular reactions in human liver: diversity at the interface. Hepatology 2011;54:1853–1863.
[3] Ryoo HD, Gorenc T, Steller H. Apoptotic cells can induce compensatory cell proliferation through the JNK and the Wingless signaling pathways. Dev Cell 2004;7:491–501.
[4] Kondo S, Senoo-Matsuda N, Hiromi Y, Miura M. DRONC coordinates cell death and compensatory proliferation. Mol Cell Biol 2006;26:7258–7268.
[5] Tait SW, Green DR. Mitochondria and cell death: outer membrane permeabilization and beyond. Nat Rev Mol Cell Biol 2010;11:621–632.
[6] Fan Y, Bergmann A. Distinct mechanisms of apoptosis-induced compensatory proliferation in proliferating and differentiating tissues in the Drosophila eye. Dev Cell 2008;14:399–410.
[7] Lackner C, Gogg-Kamerer M, Zatloukal K, Stumptner C, Brunt EM, Denk H. Ballooned hepatocytes in steatohepatitis: the value of keratin immunohistochemistry for diagnosis. J Hepatol 2008;48:821–828.
[8] Guy CD, Suzuki A, Zdanowicz M, Abdelmalek MF, Burchette J, Unalp A, et al. Hedgehog pathway activation parallels histologic severity of injury and fibrosis in human non-alcoholic fatty liver disease. Hepatology 2012;55:1711–1721.
[9] Caldwell S, Ikura Y, Dias D, Isomoto K, Yabu A, Moskaluk C, et al. Hepatocellular ballooning in NASH. J Hepatol 2010;53:719–723.
[10] Jung Y, Witek RP, Syn WK, Choi SS, Omenetti A, Premont R, et al. Signals from dying hepatocytes trigger growth of liver progenitors. Gut 2010;59:655–665.
[11] Syn WK, Choi SS, Liaskou E, Karaca GF, Agboola KM, Oo YH, et al. Osteopontin is induced by hedgehog pathway activation and promotes fibrosis progression in non-alcoholic steatohepatitis. Hepatology 2011;53:106–115.
[12] Kakisaka K, Cazanave SC, Fingas CD, Guicciardi ME, Bronk SF, Werneburg NW, et al. Mechanisms of lysophosphatidylcholine-induced hepatocyte lipoapoptosis. Am J Physiol Gastrointest Liver Physiol 2012;302:G77–84.
[13] Kuida K, Zheng TS, Na S, Kuan C, Yang D, Karasuyama H, et al. Decreased apoptosis in the brain and premature lethality in CPP32-deficient mice. Nature 1996;384:368–372.
[14] Listenberger LL, Brown DA. Fluorescent detection of lipid droplets and associated proteins. Curr Protoc Cell Biol 2007: Unit 24 2 [chapter 24].
[15] Higuchi H, Bronk SF, Bateman A, Harrington K, Vile RG, Gores GJ. Viral fusogenic membrane glycoprotein expression causes syncytia formation with bioenergetic cell death: implications for gene therapy. Cancer Res 2000;60:6396–6402.
[16] Cazanave SC, Elmi NA, Akazawa Y, Bronk SF, Mott JL, Gores GJ. CHOP and AP-1 cooperatively mediate PUMA expression during lipoapoptosis. Am J Physiol Gastrointest Liver Physiol 2010;299:G236–243.
[17] Cazanave SC, Mott JL, Elmi NA, Bronk SF, Werneburg NW, Akazawa Y, et al. JNK1-dependent PUMA expression contributes to hepatocyte lipoapoptosis. J Biol Chem 2009;284:26591–26602.
[18] Reddy JK, Hashimoto T. Peroxisomal beta-oxidation and peroxisome proliferator-activated receptor alpha: an adaptive metabolic system. Annu Rev Nutr 2001;21:193–230.
[19] Schreurs M, Kuipers F, van der Leij FR. Regulatory enzymes of mitochondrial beta-oxidation as targets for treatment of the metabolic syndrome. Obes Rev 2010;11:380–388.
[20] Rangwala F, Guy CD, Lu J, Suzuki A, Burchette JL, Abdelmalek MF, et al. Increased production of sonic hedgehog by ballooned hepatocytes. J Pathol 2011;224:401–410.
[21] Malhi H, Bronk SF, Werneburg NW, Gores GJ. Free fatty acids induce JNK-dependent hepatocyte lipoapoptosis. J Biol Chem 2006;281:12093–12101.
[22] Cazanave SC, Mott JL, Bronk SF, Werneburg NW, Fingas CD, Meng XW, et al. Death receptor 5 signaling promotes hepatocyte lipoapoptosis. J Biol Chem 2011;286:39336–39348.
[23] Eferl R, Wagner EF. AP-1: a double-edged sword in tumorigenesis. Nat Rev Cancer 2003;3:859–868.
[24] Kroemer G, Martin SJ. Caspase-independent cell death. Nat Med 2005;11:725–730.
[25] Han ME, Lee YS, Baek SY, Kim BS, Kim JB, Oh SO. Hedgehog signaling regulates the survival of gastric cancer cells by regulating the expression of Bcl-2. Int J Mol Sci 2009;10:3033–3043.
[26] Syn WK, Jung Y, Omenetti A, Abdelmalek M, Guy CD, Yang L, et al. Hedgehog-mediated epithelial-to-mesenchymal transition and fibrogenic repair in non-alcoholic fatty liver disease. Gastroenterology 2009;137:1478–1488, e1478.
[27] Shin K, Lee J, Guo N, Kim J, Lim A, Qu L, et al. Hedgehog/Wnt feedback supports regenerative proliferation of epithelial stem cells in bladder. Nature 2011;472:110–114.
[28] Regl G, Kasper M, Schnidar H, Eichberger T, Neill GW, Philpott MP, et al. Activation of the BCL2 promoter in response to Hedgehog/GLI signal transduction is predominantly mediated by GLI2. Cancer Res 2004;64:7724–7731.
[29] Walterhouse DO, Yoon JW, Iannaccone PM. Developmental pathways: sonic hedgehog-Patched-GLI. Environ Health Perspect 1999;107:167–171.
[30] Mahindroo N, Punchihewa C, Fujii N. Hedgehog–Gli signaling pathway inhibitors as anticancer agents. J Med Chem 2009;52:3829–3845.
[31] Malhi H, Guicciardi ME, Gores GJ. Hepatocyte death: a clear and present danger. Physiol Rev 2010;90:1165–1194.
[32] Masuoka HC, Mott J, Bronk SF, Werneburg NW, Akazawa Y, Kaufmann SH, et al. Mcl-1 degradation during hepatocyte lipoapoptosis. J Biol Chem 2009;284:30039–30048.
[33] Alkhouri N, Dixon LJ, Feldstein AE. Lipotoxicity in non-alcoholic fatty liver disease: not all lipids are created equal. Expert Rev Gastroenterol Hepatol 2009;3:445–451.
[34] Monetti M, Levin MC, Watt MJ, Sajan MP, Marmor S, Hubbard BK, et al. Dissociation of hepatic steatosis and insulin resistance in mice overexpressing DGAT in the liver. Cell Metab 2007;6:69–78.
[35] Listenberger LL, Han X, Lewis SE, Cases S, Farese Jr RV, Ory DS, et al. Triglyceride accumulation protects against fatty acid-induced lipotoxicity. Proc Natl Acad Sci U S A 2003;100:3077–3082.
[36] Fan Y, Bergmann A. Apoptosis-induced compensatory proliferation. The Cell is dead. Long live the Cell! Trends Cell Biol 2008;18:467–473.
[37] Wells BS, Yoshida E, Johnston LA. Compensatory proliferation in Drosophila imaginal discs requires Dronc-dependent p53 activity. Curr Biol 2006;16:1606–1615.
[38] Witek RP, Stone WC, Karaca FG, Syn WK, Pereira TA, Agboola KM. Pan-caspase inhibitor VX-166 reduces fibrosis in an animal model of non-alcoholic steatohepatitis. Hepatology 2009;50:1421–1430.
[39] Yimin, Furumaki H, Matsuoka S, Sakurai T, Kohanawa M, Zhao S, et al. A novel murine model for non-alcoholic steatohepatitis developed by combination of a high-fat diet and oxidized low-density lipoprotein. Lab Invest 2012;92:265–281.